LANGMUIR

pubs.acs.org/Langmuir Article

Size Effect of Platinum Nanoparticles over Platinum−Manganese Oxide on the Low-Temperature Oxidation of Toluene

Lixin Zhang, Linjun Zhong, Pinhua Yu, Haitao Li, Zhou Zhou, Qing Tong, Haiqin Wan,* and Lin Dong

Cite This: *Langmuir* 2023, 39, 13620−13629 Read Online

ACCESS | Metrics & More | Article Recommendations | Supporting Information

ABSTRACT: The effect of size of Pt nanoparticles has an important influence on the performance of supported Pt-based catalysts for the elimination of toluene. Herein, uniform Pt nanoparticles with average sizes of 1.5, 2.0, 2.5, 2.9, and 3.6 nm were obtained and supported on manganese oxide octahedral molecular sieves (OMS-2), and their catalytic performances for toluene oxidation were evaluated. Benefiting from the moderate interfacial interaction between nanoparticles and manganese oxide support, Pt/OMS-2−3 with the Pt particle size of 3.0 nm showed the best catalytic performance owing to the highest content of Pt^{2+} species. It also facilitates the formation of more abundant $Mn^{\delta+}$ (Mn^{2+} and Mn^{3+}) and oxygen vacancies than that of the other sizes of the OMS-2-supported Pt nanoparticles, which can be filled by a large amount of adsorbed oxygen and converted into reactive oxygen species. We further showed that the resulting surface synergetic oxygen vacancies (Pt^{2+}−O_v−$Mn^{\delta+}$) play a decisive part in catalyzing the complete oxidation of toluene. The result will provide new insights for designing efficient Pt-based catalysts for deep purification of toluene.

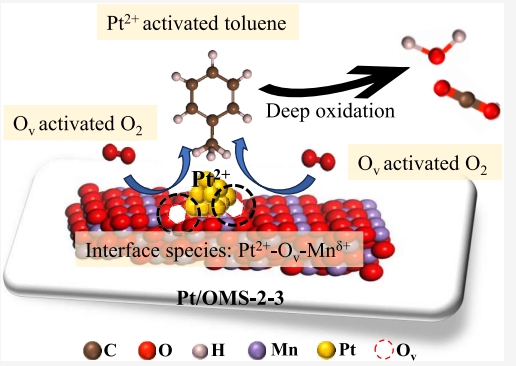

INTRODUCTION

Recently, the emissions of volatile organic compounds (VOCs) have increased with the acceleration of industrialization and urbanization, as well as the continuous growth of energy consumption.[1,2] Toluene is considered one of the typical VOCs because it is commonly used as a solvent and additive in petrochemical and other productive processes. Long-term exposure to toluene poses a serious threat to human health, causing diseases of the nervous system, respiratory tract, and immune function.[3] It would lead to serious atmospheric pollution through the formation of secondary organic aerosols and photochemical smog. Therefore, many effective technologies have been developed for the purification and elimination of toluene, such as adsorption, membrane separation, biodegradation, plasma, photocatalytic removal, and catalytic oxidation.[4−6] Among them, catalytic oxidation has attracted vast attention due to its low energy consumption, high treatment efficiency, and absence of secondary pollution.[7] Therefore, the reasonable design of efficient and practical catalysts for low-temperature toluene removal is of great significance.

Among various catalysts, Pt-based catalysts have been widely used in laboratory research and various complex working conditions due to their excellent catalytic activity and stability.[8,9] However, in view of the high cost and limited reserves of precious metals, how to construct a highly efficient Pt-based catalyst at a low noble loading has been a hot topic in VOC oxidation.[10,11] Various approaches have been developed for the precise structural regulation of Pt-based catalysts such as Pt particle size, surface valence state, and the strength of the interaction between Pt and support.[11−17] Among them, the size effect of Pt has always been an important topic, which has been shown to significantly affect the catalytic activity.[11−13] Peng et al.[17] used the Pt/CeO_2 as a model catalyst and investigated the size effect of Pt nanoparticles for toluene oxidation. They found that the catalyst Pt/CeO_2-1.8 showed the best performance owing to the equilibrium between the concentration of oxygen vacancy on CeO_2 and the dispersion of Pt. It is worth noting that the size effect is not independent, and the regulation of Pt size and dispersity can significantly alter the surface chemical state.[14] The surface valence state of Pt has been considered to have a crucial impact on the active site. Although many studies are expected to clarify the effects of metallic and oxidized Pt on toluene adsorption and oxygen activation, the role of Pt^0 and $Pt^{\delta+}$ in toluene oxidation is still not conclusive for specific catalysts.[18,19] Meanwhile, the result suggests that the strength of strong metal−support interaction (SMSI) is different depending on the valence state of Pt, and the special role of SMSI in the reaction cannot be ignored, which is worthy of further study.[20]

Received: June 27, 2023
Revised: August 30, 2023
Published: September 13, 2023

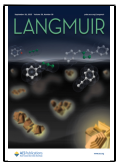

https://doi.org/10.1021/acs.langmuir.3c01734
Langmuir 2023, 39, 13620−13629

Previously, we proved that the surface synergistic oxygen vacancy (SSOV) (−Cu−□−Mn−) over the $CuO/Mn_2O_3/Al_2O_3$ catalyst was the key active site in the NO + CO reaction.[21] The structure has also been confirmed on $CuO-V_2O_5/\gamma\text{-}Al_2O_3$, CuO_x-CeO_2, and Fe/CeO_2 catalysts.[22−24] Recently, it has been reported that the SSOV structure also exists on noble metal catalysts. Yan et al.[25] obtained a Pt/TiO_2-C catalyst with a $Ti^{\delta+}-Vo^{\bullet}-Pt^{\delta+}$ interface structure, which accelerated the preactivation of toluene to generate a large number of reactive intermediates for photocatalytic reactions. In our previous work, $Pt^{2+}-Vo-Mn^{\delta+}$ species was the major active site for the oxidation of toluene.[26] Thus, the formation of SSOV structures could facilitate catalytic reactions.

On this basis, we produced a series of uniform Pt nanoparticles with controllable size by changing the molar ratio of NaOH to Pt in the ethylene glycol reduction method.[27] The manganese oxide with an octahedral molecular sieve structure was selected as the support. By adjusting the Pt size, the surface chemical state of Pt and the interfacial interaction on $Pt-MnO_2$ were regulated to optimize the surface synergistic oxygen vacancies and improve the combustion performance of toluene on the Pt/OMS-2 catalyst.

EXPERIMENTAL SECTION

Materials. Potassium permanganate ($KMnO_4$), acetic acid, manganese acetate tetrahydrate ($MnAc_2{\cdot}4H_2O$), chloroplatinic acid hexahydrate ($H_2PtCl_6{\cdot}6H_2O$), poly(vinylpyrrolidone) (PVP), and ethylene glycol were analytical grade and used without further purification. The detailed produced companies are described in the Supporting Information.

Preparation of Catalysts. The Pt/OMS-2 catalysts were prepared in two steps.[26] The detailed description is presented in the Supporting Information. The particle sizes of Pt were tuned by the molar ratio of NaOH to Pt, and the corresponding Pt sizes are tabulated in Table 1. The obtained sample was denoted as Pt/OMS-2-*x* (*x* represents the Pt particle size).

Table 1. Pt Particle Size and Dispersion of the Catalysts

catalyst	molar ratio of NaOH/Pt	Pt particle size (nm)	D_{TEM} (%)	D_{CO} (%)
Pt/OMS-2−1.5	12.5	1.52 ± 0.02	74.0	71.2
Pt/OMS-2−2	10.0	2.08 ± 0.02	54.1	50.4
Pt/OMS-2−2.5	6.5	2.51 ± 0.02	44.8	35.1
Pt/OMS-2−3	5.5	2.92 ± 0.03	38.5	29.2
Pt/OMS-2−3.5	4.8	3.64 ± 0.03	30.8	22.5

Catalyst Characterizations. Physicochemical properties of the as-prepared samples were characterized using the following techniques, including X-ray diffraction (XRD), N_2 adsorption−desorption (BET), transmission electron microscopy (TEM), CO pulse chemisorption, X-ray photoelectron spectroscopy (XPS), Raman spectra, hydrogen-temperature-programmed reduction (H_2-TPR), oxygen-temperature-programmed desorption (O_2-TPD), toluene-temperature-programmed desorption (toluene-TPD), and *in situ* diffuse reflectance infrared Fourier transform spectroscopy (*in situ* DRIFTS). The detailed procedures are described in the Supporting Information.

Catalytic Activity Test. The catalytic performance of Pt/OMS-2-*x* for toluene oxidation was tested in a continuous flow fixed-bed microreactor with a WHSV of 30 000 $mL{\cdot}g^{-1}{\cdot}h^{-1}$. Typically, 100 mg of catalyst (20−40 mesh) was used, a 1000 ppm toluene balance with air was the reactant, and the reaction products were detected and analyzed by gas chromatography (GC) equipped with a flame ionization detector (FID) and a thermal conductivity detector (TCD). Three parallel tests were performed and averaged to evaluate the performance of each catalyst. The detailed calculation methods of toluene conversion, the turnover frequency (TOF), and the apparent activation energy (Ea) are listed in the Supporting Information.

RESULTS AND DISCUSSION

Morphology and Structure of Catalysts. The morphology and particle size distribution of the catalysts were first investigated by TEM (Figures 1 and S1 and Table 1). As shown in Figure S1, simple OMS-2 displayed a one-dimensional nanorod structure with a diameter of 10−20 nm and length ranging from a few tens to hundred nanometers.[28] After the deposition of Pt nanoparticles, all Pt/OMS-2-*x* catalysts still maintained uniform rod-shaped morphology with a homogeneous distribution of Pt particles on the surface of the support. The average particle size and distribution were obtained based on the measurement of at least 200 Pt particles. As shown in Table 1, the average particle size of the Pt species increased significantly from 1.52 to 3.64 nm as the NaOH/Pt ratio decreased, with an obvious normal distribution obtained in the size distribution histograms of each sample. The dispersion of Pt was calculated according to the particle size and CO pulse chemisorption.

The XRD patterns of various catalysts displayed the same structure as the OMS-2 support (JCPDS PDF No. 44-0141) (Figure 2),[29] with no characteristic diffraction peaks of Pt species detected, further evidencing the small size of Pt nanoparticles. The N_2 adsorption−desorption isotherm and BJH pore size distribution curves of all samples displayed a type IV isotherm with an H_3 hysteresis loop, indicating the existence of piled mesopores in the catalysts (Figure S2). It was found that after the deposition of different Pt sizes on the OMS-2, the structure of catalysts remained intact with no significant changes in the specific surface area, pore volume, or average pore diameter (Table S1).

Surface Chemical States and Redox Properties of Catalysts. Raman spectroscopy was carried out to investigate the effect of Pt loading on the surface bonding and structure of catalysts. As shown in Figure S3, the strong vibration band near 640 cm^{-1} was attributed to lattice symmetric stretching vibration (Mn−O) perpendicular to the double-chain direction of the MnO_6 octahedron, while the vibration peak near 350 cm^{-1} was attributed to the planar bending vibration mode (Mn−O−Mn).[30] With the introduction of Pt, the peaks become significantly weakened and widened, indicating the fracture of some Mn−O bonds and the enhancement of oxygen mobility, which could induce the formation of more oxygen defects.[31]

In order to explore the trend of surface chemical state and interfacial interaction of supports with increasing size of Pt nanoparticles, the samples were characterized by XPS. The Mn $2p_{3/2}$ XPS results of all samples are shown in Figure 3a. The three main peaks near 640.6−640.7, 641.9−642.3, and 643.3−643.7 eV were attributed to Mn^{2+}, Mn^{3+}, and Mn^{4+} species, respectively.[32] Interestingly, with the increase of Pt particle size, the molar ratio of low-valence Mn (Mn^{2+} + Mn^{3+}) to Mn^{4+} ((Mn^{2+} + Mn^{3+})/Mn^{4+}) first increased and then decreased, with the maximum value obtained for the Pt/OMS-2−3 catalyst ((Mn^{2+} + Mn^{3+})/Mn^{4+} = 2.26) (Table 2). Alternatively, the average oxidation state (AOS) of Mn was also calculated based on the binding energy difference of Mn 1s doublets (ΔE_s), with lower AOS values representing the higher concentration of low-valence Mn (Figure 3b).[33,34] As

https://doi.org/10.1021/acs.langmuir.3c01734
Langmuir 2023, 39, 13620−13629

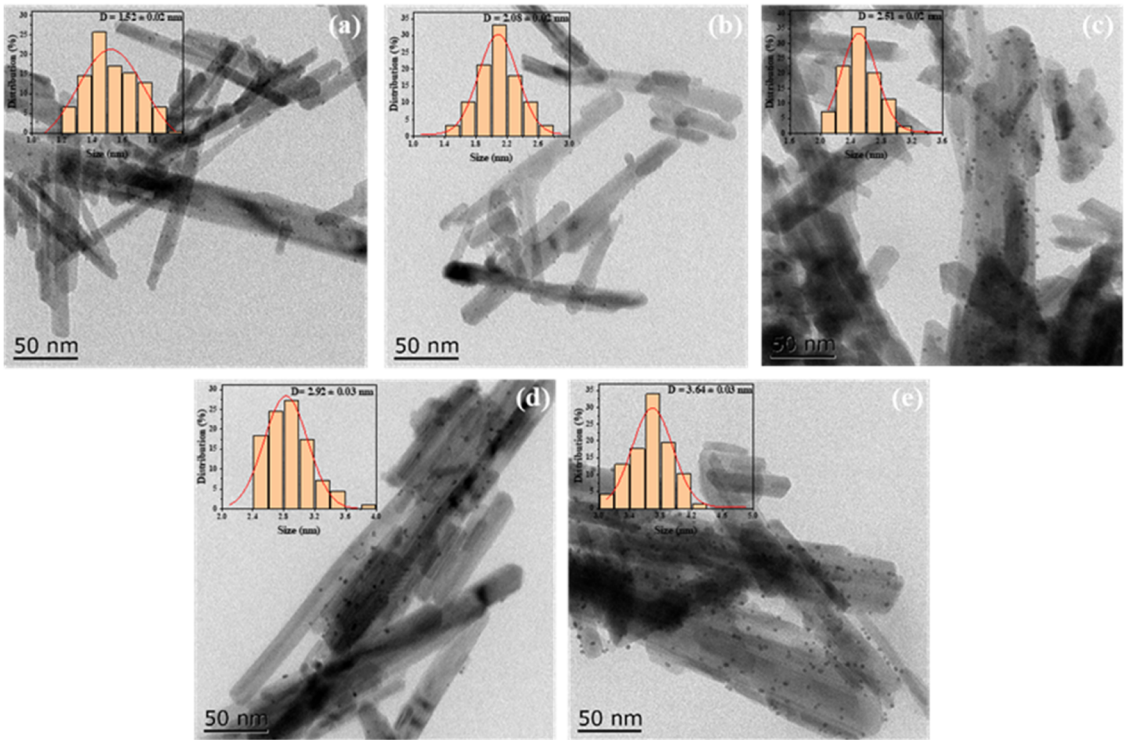

Figure 1. TEM images of the catalysts and the corresponding particle size distribution histograms of Pt: (a) Pt/OMS-2−1.5, (b) Pt/OMS-2−2, (c) Pt/OMS-2−2.5, (d) Pt/OMS-2−3, and (e) Pt/OMS-2−3.5.

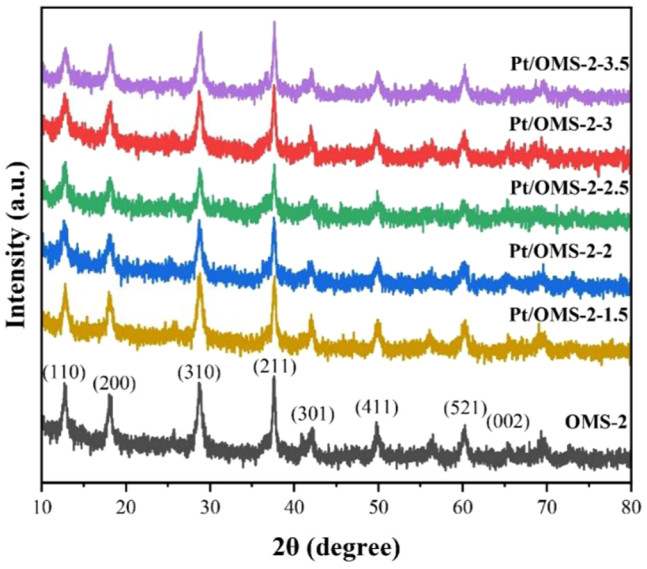

Figure 2. XRD patterns of various Pt/OMS-2 and OMS-2 samples.

shown in Table 2, the AOS values of various catalysts followed the sequence of Pt/OMS-2−3 < Pt/OMS-2−2.5 < Pt/OMS-2−3.5 < Pt/OMS-2−2 < Pt/OMS-2−1.5, in good agreement with the XPS analysis of the Mn 2p region.

Figure 3c shows the O 1s XPS spectra of all catalysts. Three peaks could be observed in each sample, which were attributed to surface lattice oxygen (ca. 529.7 eV, denoted as O_{latt}), surface chemisorbed oxygen (ca. 531.1 eV, denoted as O_{ads}), and surface hydroxyl oxygen (ca. 532.6 eV, denoted as OH).[35] The molar ratio of O_{ads}/O_{total} was of the order of Pt/OMS-2−3 (18.9%) > Pt/OMS-2−2.5 (18.1%) > Pt/OMS-2−3.5 (17.3%) > Pt/OMS-2−2 (17.0%) > Pt/OMS-2−1.5 (15.8%). This trend was well consistent with the order of concentration of low-valence Mn, as lower oxidation states of Mn induce decreased coordination of O to Mn, which promotes the formation of O vacancies.[33] In general, the replenishment and activation of oxygen vacancies by adsorbed oxygen was proven to be a necessary condition for the oxidation reaction.[33] Therefore, the high content of low-valence Mn and O_{ads} in Pt/OMS-2−3 might be conducive to catalytic combustion of toluene, similar results were reported by Yang et al. and Wang et al.[36,37]

In this work, the surface chemical state of Pt and interfacial interaction were also regulated by changing the Pt size. As shown in Figure 3d, the Pt 4f XPS spectra of the catalysts were divided into three doublets with Pt $4f_{7/2}$ binding energies at 71.6, 72.5, and 74.3 eV, which were assigned to Pt^0, Pt^{2+}, and Pt^{4+}, respectively.[38] In general, smaller Pt nanoparticles contained a higher percentage of surface Pt atoms that are at the interface of OMS-2 and Pt nanoparticles, resulting in stronger interaction between metal and support and thereby higher content of Pt^{4+}.[39,40] As expected, the surface concentration of Pt^{4+} increased, and Pt^0 decreased with the shrinking Pt particle size, indicating that the chemical state of Pt was indeed affected by the dimension of Pt nanoclusters. Besides the strong (Pt^{4+}) and weak (Pt^0) metal−support interactions, a media strength of metal−support interaction existed on the surface of Pt/OMS-2, which is Pt^{2+} species.[12] It was worth noting that the concentration of Pt^{2+} also showed a volcano-shaped relationship with Pt particle size, with the maximum Pt^{2+} percentage obtained on Pt/OMS-2−3, indicating that it had the most Pt species with a media strength of metal−support interaction due to the proper size. On the basis of the aforementioned XPS results that Pt/OMS-2−3 had the highest concentration of low-valence Mn species (Mn^{2+} and Mn^{3+}, denoted as $Mn^{\delta+}$), oxygen vacancies (O_v),

https://doi.org/10.1021/acs.langmuir.3c01734
Langmuir 2023, 39, 13620−13629

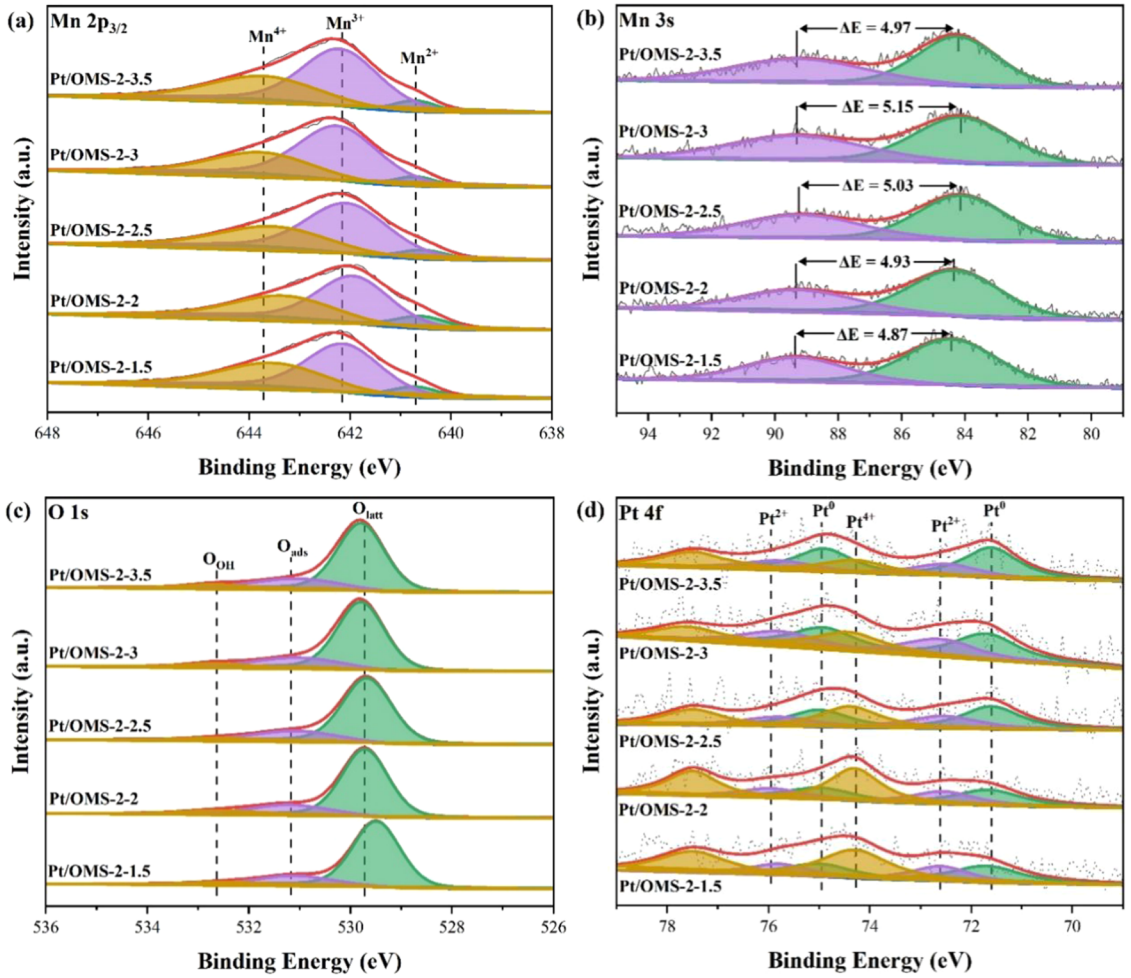

Figure 3. (a) Mn $2p_{3/2}$, (b) Mn 3s, (c) O 1s, and (d) Pt 4f XPS spectra for the as-prepared Pt-based samples.

Table 2. XPS Results of the Catalysts

catalyst	$(Mn^{2+} + Mn^{3+})/Mn^{4+}$	AOS[a]	O_{ads}/O_{total} (%)	Pt^0/Pt_{total} (%)	Pt^{2+}/Pt_{total} (%)	Pt^{4+}/Pt_{total} (%)
Pt/OMS-2−1.5	1.72	3.48	15.8	29.0	22.2	48.8
Pt/OMS-2−2	1.92	3.41	17.0	30.1	23.1	46.8
Pt/OMS-2−2.5	2.05	3.29	18.1	38.6	25.7	35.7
Pt/OMS-2−3	2.26	3.16	18.9	41.6	30.5	27.9
Pt/OMS-2−3.5	1.96	3.36	17.3	51.4	23.8	24.8

[a]AOS = 8.956 − 1.126 ΔE_s (eV).

and Pt^{2+} species, it is reasonable to propose that Pt/OMS-2−3 contained more $Pt^{2+}-O_v-Mn^{\delta+}$ surface synergetic oxygen vacancies (SSOVs) at the interface than other catalysts.[21,23]

An H_2-TPR experiment was then performed to further investigate the relationship between the size of Pt clusters and the strength of strong metal−support interaction (SMSI) at the interface of the catalysts. As shown in Figure 4a, all samples showed three peaks in the range of 50−450 °C, which was divided into regions I and II. The reduction peaks of 100−220 °C in region I were attributed to the reduction of surface Pt species (Pt−O) and surface Mn^{3+} or Mn^{4+} with strong interactions with Pt (Pt−O−Mn), while the reduction peak in region II was attributed to the multistep reduction of $Mn^{4+} \rightarrow Mn^{3+} \rightarrow Mn^{2+}$.[41] As the Pt size increases, the reduction temperature of the peak decreases first and then increases, with Pt/OMS-2−3 showing the lowest reduction temperature at 102 °C, suggesting a strong dependence of reduction temperature on particle size. The hydrogen consumptions of the peak in region I on Pt/OMS-2−1.5, −2, −2.5, −3, and −3.5 catalysts were quantitatively determined to be 8.07, 7.64, 7.15, 6.83, and 6.45 mmol·g^{-1}, respectively. Combined with the XPS results, for smaller-sized Pt nanoparticles supported on OMS-2, larger hydrogen consumption manifested higher Pt^{4+} content in the catalyst and stronger SMSI at the Pt−MnO_2 interface.[40] However, excessively strong interaction at the interface might stabilize lattice oxygen and hinder the migration of oxygen species, making it more difficult to be reduced by H_2, and thus showing a higher reduction temperature.[42] In addition, it was noted that Pt/OMS-2−3.5 had the lowest hydrogen consumption, indicating that this weak interaction resulted in relatively less formation of Pt−O−Mn structures, and Pt species were less reactive and could not be easily reduced. The low-temperature reducibility of samples could be evaluated using the initial H_2 consumption rate

https://doi.org/10.1021/acs.langmuir.3c01734
Langmuir 2023, 39, 13620−13629

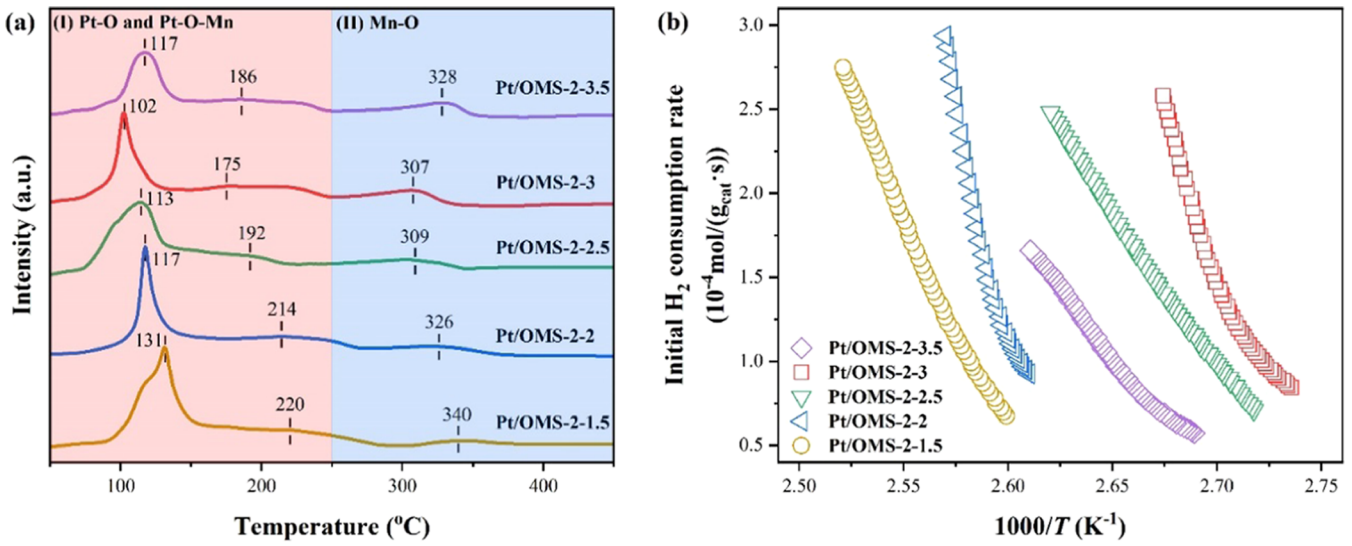

Figure 4. (a) H_2-TPR profiles and (b) initial H_2 consumption rate versus the inverse temperature of all samples.

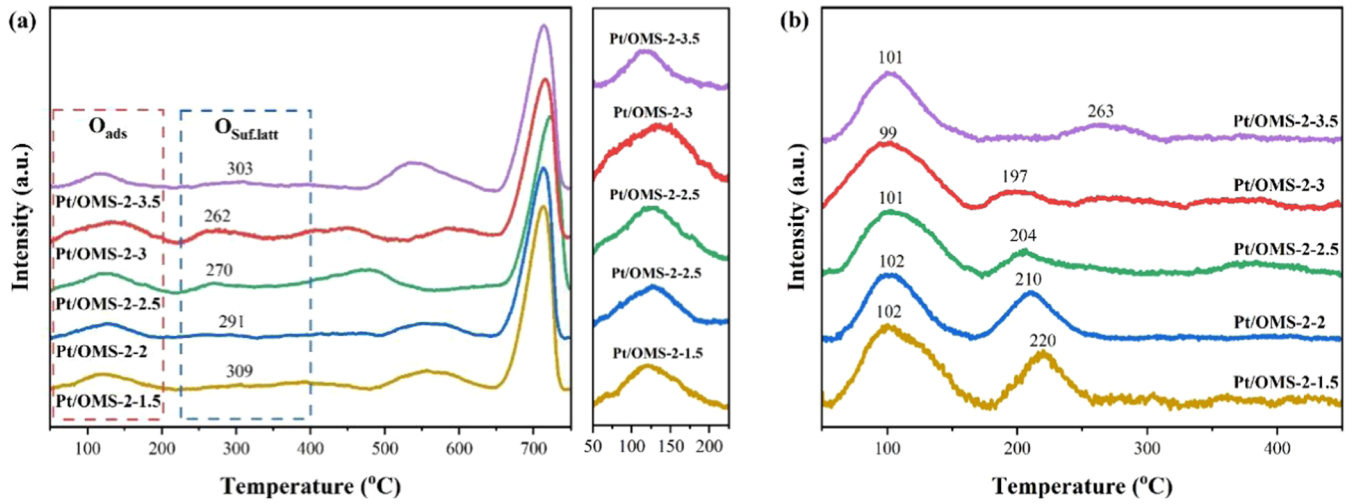

Figure 5. (a) O_2-TPD and (b) toluene-TPD profiles of the Pt/OMS-2 samples.

(where less than 25% oxygen for the first reduction peak of the sample is removed).[43] Figure 4b shows that the initial hydrogen consumption rate followed the order of Pt/OMS-2−3 > Pt/OMS-2−2.5 > Pt/OMS-2−3.5 > Pt/OMS-2−2 > Pt/OMS-2−1.5, which was in good agreement with the content of $Mn^{\delta+}$, O_{ads}, and Pt^{2+} obtained from XPS analysis. These results indicated that the strength of SMSI could be regulated by controlling the size of Pt nanoparticles, with the moderate SMSI on Pt/OMS-2−3 generating more $Pt^{2+}-O_v-Mn^{\delta+}$ structures than other materials.

O_2-TPD characterization was conducted to investigate the effect of the size of Pt nanoparticles on the oxygen species in the Pt/OMS-2 catalyst. As shown in Figure 5a, the desorption peak of 100−200 °C was attributed to surface-adsorbed oxygen species (O_{ads}), which could quickly participate in the combustion of toluene due to its weak binding with the surface.[26] The desorption peak at 250−400 °C was assigned to surface lattice oxygen species (O_{latt}), which resulted from the breaking of Mn−O and Pt−O−Mn bonds, and the desorption peak at 500−750 °C was assigned to bulk lattice oxygen species.[44] A closer examination of the profile within the range of 100−200 °C showed that Pt/OMS-2−3 possessed more O_{ads} species, a lower desorption temperature of surface lattice oxygen, and a higher peak intensity. Furthermore, the peak corresponding to the breaking of bulk lattice oxygen also shifted toward a lower temperature.[45] The above observations indicated that the mobility of surface lattice oxygen was significantly enhanced after loading 3 nm of Pt, resulting in more SSOV structures of $Pt^{2+}-O_v-Mn^{\delta+}$ and improved migration of abundant oxygen from the bulk phase to the surface or subsurface than other samples.

In order to explore the adsorption and activation ability of Pt/OMS-2 samples to toluene, a toluene-TPD experiment was carried out. Figure 5b shows that two peaks could be observed on all catalysts, and one peak near 100 °C was attributed to the physical adsorption of toluene on the catalyst, which could be desorbed at low temperatures.[38] The desorption peak at 197−263 °C was attributed to the desorption of CO_2, indicating that toluene was further oxidized to CO_2 by the active site due to the stronger interaction between the chemisorbed toluene and the catalyst.[46] It was a remarkable fact that Pt/OMS-2−3 had the lowest desorption temperature, which indicated that Pt/OMS-2−3 could adsorb toluene quickly and enhance the deep activation of toluene at lower temperatures. In addition, with

https://doi.org/10.1021/acs.langmuir.3c01734
Langmuir 2023, 39, 13620−13629

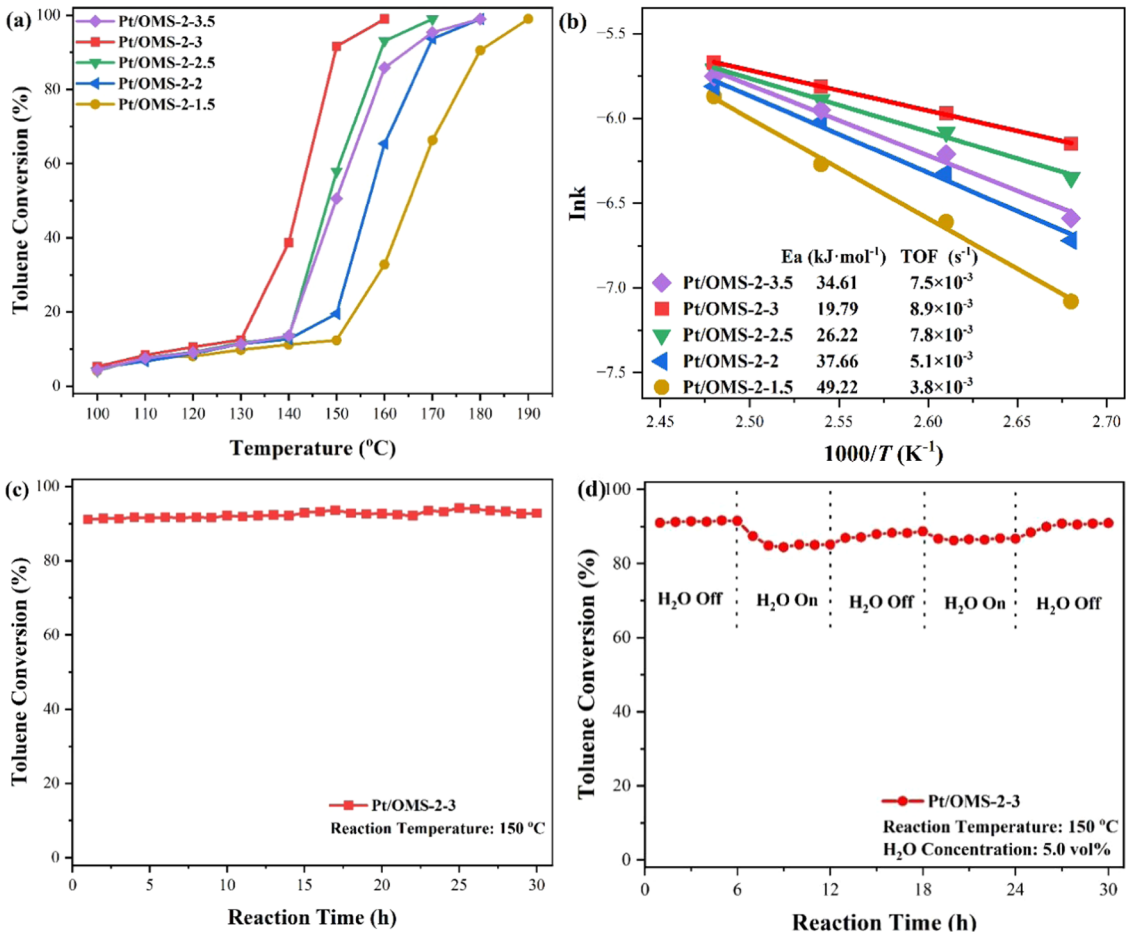

Figure 6. (a) Conversion of toluene and (b) Arrhenius plots for the oxidation of toluene over different Pt/OMS-2 catalysts. (c) Stability of the Pt/OMS-2−3 catalyst at 150 °C. (d) Effect of water vapor on toluene conversion at 150 °C over the Pt/OMS-2−3 catalyst.

the decrease of the Pt size, the desorption peak of toluene moved toward a higher temperature, and the peak strength increased obviously, which was due to the strong adsorption of toluene by high-valence Pt. However, such a strong adsorption might lead to excessive accumulation of toluene on the catalyst surface and covering the active site, which was not conducive to further oxidation of toluene.[47,48] Combining the results of XPS and O_2-TPD, more surface synergetic oxygen vacancies could promote the generation of more reactive oxygen species and the desorption and further activation of toluene.

Catalytic Activity. The catalytic combustion curves of all Pt/OMS-2 samples shown in Figure 6a suggest that the catalytic activity exhibits an obvious dependence on the size of Pt nanoparticles. As the Pt particle size increased, the conversion temperature first decreased and then increased. Pt/OMS-2−3 showed the best catalytic oxidation activity for toluene, achieving a high conversion rate of over 90% for toluene oxidation at 150 °C. The reaction kinetics of various catalysts were evaluated in terms of the turnover frequency (TOF) of Pt. The order of the TOF_{Pt} value was as follows: Pt/OMS-2−3 > Pt/OMS-2−2.5 > Pt/OMS-2−3.5 > Pt/OMS-2−2 > Pt/OMS-2−1.5. Figure 6b shows the apparent activation energies (E_a) of various catalysts measured under low toluene conversion according to the Arrhenius equation. The sequence of E_a values was Pt/OMS-2−3 (19.79 kJ·mol^{-1}) < Pt/OMS-2−2.5 (26.22 kJ·mol^{-1}) < Pt/OMS-2−3.5 (34.61 kJ·mol^{-1}) < Pt/OMS-2−2 (37.66 kJ·mol^{-1}) < Pt/OMS-2−1.5 (49.22 kJ·mol^{-1}). The lowest E_a value of Pt/OMS-2−3 indicated that the oxidation reaction of toluene was the most easily activated, which was consistent with the activity results.

The thermal stability of the most active Pt/OMS-2−3 was then tested at the reaction temperature of 150 °C. As shown in Figure 6c, the Pt/OMS-2−3 catalyst displayed excellent stability and maintained a high toluene conversion rate for 30 h. In addition, in the actual industrial environment, the presence of water vapor usually could not be ignored. In this study, the water-resistant cyclic toluene oxidation experiment of Pt/OMS-2−3 was conducted for 30 h by alternately switching on/off 5 vol % water vapor at 150 °C. As shown in Figure 6d, the catalytic activity decreased slightly after the introduction of water vapor, but gradually recovered after water vapor was turned off.[49] The excellent catalytic activity, long-term thermal stability, and water resistance toward toluene removal endowed the Pt/OMS-2−3 catalyst with good application prospects. To investigate the change of the catalyst during the reaction, the TEM and XPS spectra of Pt/OMS-2−3 after the reaction were characterized and compared with the fresh sample. As shown in Figure S4, the average size of Pt nanoparticles (2.87 nm) was close to that of the fresh sample (2.92 nm). From Figure S5 and Table S2, it could be found that the proportion of each state of Mn, O, and Pt species varied, such as a decrease in the lower-valence Mn (Mn^{2+}/Mn^{3+}) and Pt^{2+}, while an increase in adsorbed oxygen and Pt^0 and Pt^{4+}, suggesting that the interface species Pt^{2+}−O_v−$Mn^{\delta+}$ involved toluene oxidation.

https://doi.org/10.1021/acs.langmuir.3c01734
Langmuir 2023, 39, 13620−13629

Reaction Mechanism. In order to further understand the reaction pathway of toluene oxidation, the intermediates of the reaction process were studied by *in situ* DRIFTS experiments. As shown in Figure 7, the vibration peaks at 3500−4000 cm^{-1} were attributed to separated or polymerized hydroxyl groups or adsorbed water molecules ν(O−H). The vibration peaks of the CO_2 gas phase were near 2341 and 2360 cm^{-1}.[50] The bands at 1743 and 1733 cm^{-1} were assigned to the ν(C═O) stretching vibrations of benzaldehyde, while 1698 cm^{-1} was short-chain aldehydes (such as acetaldehyde).[51] For the bands of 1671, 1649, 1635, and 1620 cm^{-1}, they were attributed to the ν(COO) stretching vibrations of benzoic acid, which was the main intermediate of toluene oxidation.[52,53] Apparently, the skeleton vibration mode of ν(C═C) was detected at 1595 and 1489 cm^{-1}, indicating the presence of aromatic ring.[50] The bands around 1520−1558, 1396, 1362, and 1340 cm^{-1} were attributed to asymmetric and symmetric ν(COO) stretching vibrations of carboxylate and carbonate species.[54] It was noteworthy that the peaks at 1506 and 1434 cm^{-1} were derived from the key intermediates of the fracture of the aromatic ring, called short-chain maleic anhydrides.[55] The vibration peak at 1068 cm^{-1} was ascribed to the ν(C−O) stretching vibration mode of benzyl alcohol species.[54]

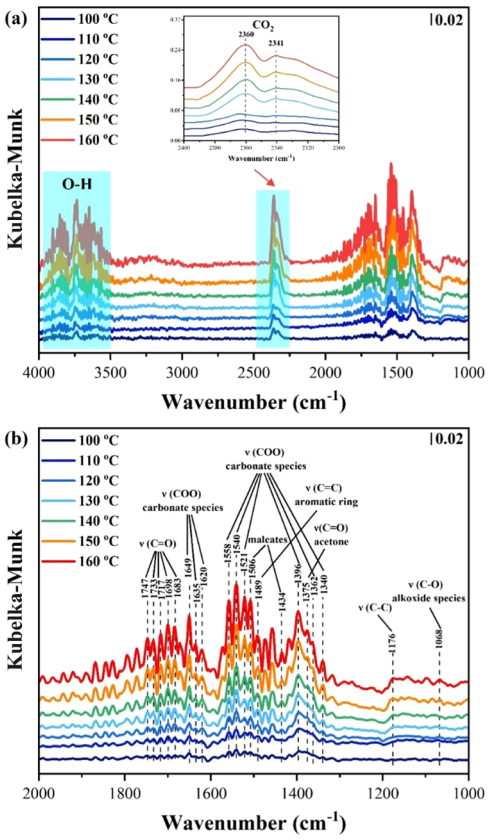

Figure 7. (a, b) *In situ* DRIFTS of toluene oxidation on a Pt/OMS-2−3 catalyst under different temperatures.

Figures 7 and S6 show the temperature-dependent *in situ* DRIFTS experiments of toluene oxidation over Pt/OMS-2−3 and Pt/OMS-2−2 catalysts, and significant differences between the two samples could be observed. First, the vibration peaks of the CO_2 gas phase and benzoate species had been detected on Pt/OMS-2−3 samples, indicating that the toluene could be partially oxidized at lower temperatures. At the same time, the vibration band intensities of benzoate and CO_2 (2341 and 2360 cm^{-1}) increased with the increase in temperature. During this process, toluene was still not completely oxidized, and reactive oxygen species participated in the catalytic reaction. It was noteworthy that the vibration bands of the maleic anhydride species, an important intermediate of aromatic ring fracture, were clearly observed at 140 °C. The vibration peak at 1375 cm^{-1} attributed to acetone was also detected, indicating that the benzene ring was destroyed and further oxidized to the short-chain aldehyde/ketone species.[56] However, for Pt/OMS-2−2, significant changes in the characteristic vibration peaks of CO_2 were observed at higher temperatures, and the intensity of the peaks was also lower than that of Pt/OMS-2−3, and the open-ring of toluene was not observed until 160 °C. Compared with Pt/OMS-2−2, Pt/OMS-2−3 with a Pt particle size of 3 nm had significant advantages in the open-ring step. The results showed that the Pt/OMS-2−3 sample was more able to catalyze the combustion of toluene and achieve the complete elimination of toluene. As shown in Figure 8, by adjusting the size of Pt, the Pt/OMS-2−3 catalyst produced the most Pt^{2+}, and the presence of $Mn^{\delta+}$ implied the generation of more oxygen vacancies, resulting in the formation of the SSOV structure

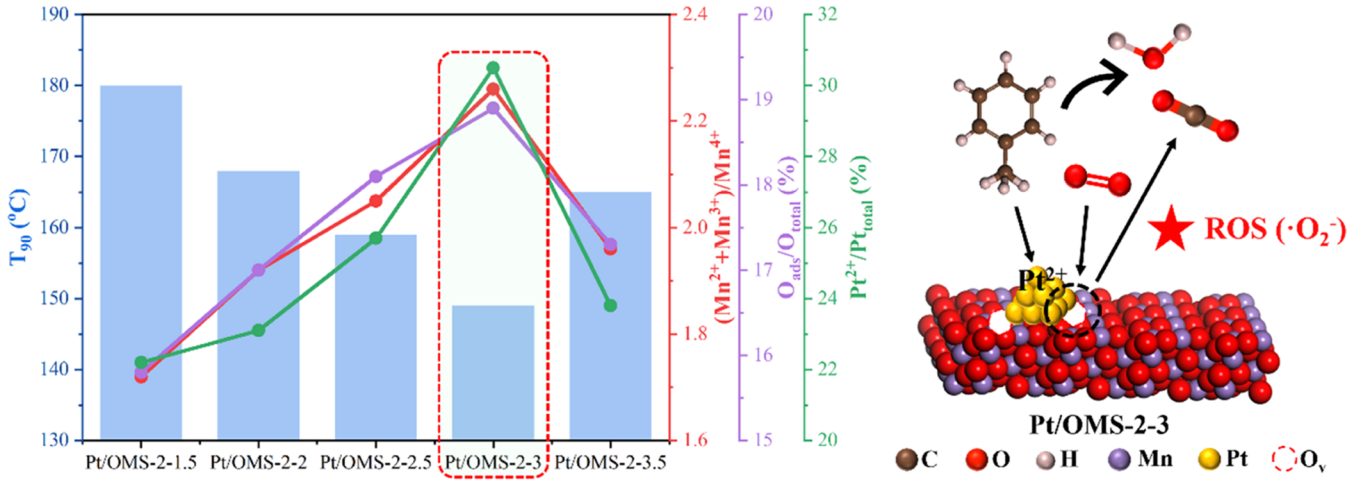

Figure 8. Proposed reaction pathway of toluene oxidation over the Pt/OMS-2−3 catalyst.

https://doi.org/10.1021/acs.langmuir.3c01734
Langmuir 2023, 39, 13620−13629

(Pt^{2+}−O_v−$Mn^{\delta+}$), on the Pt−MnO_2 interface, which played a decisive role in the reaction. Based on the results of *in situ* DRIFTS experiments of toluene, it could be concluded that the deep oxidation of toluene on Pt/OMS-2 followed the Mars−van Krevelen (MvK) mechanism.[57] Toluene was first adsorbed on the surface of the catalyst, and Pt^{2+} and Pt^{4+} were the main adsorption sites. Pt^{2+} could better promote the desorption, and intermediates, such as benzoate, were formed. More gaseous oxygen was filled in the surface synergetic oxygen vacancies and converted into activated oxygen species, thus triggering the open-ring step in the toluene oxidation process; finally, toluene was completely oxidized into CO_2 and H_2O.

CONCLUSIONS

In this work, 1.5−3.5 nm sized controllable uniform Pt nanoparticles with controllable sizes from 1.5 to 3.5 nm were obtained by adjusting the molar ratio of NaOH to Pt by using an ethylene glycol (EG) reduction method. Systematic characterizations have demonstrated that the regulation of Pt size would affect the surface chemical valence of Pt and a strong metal−support interaction. The presence of the most Pt^{2+} on the Pt/OMS-2−3 catalyst of 3 nm indicated the generation of moderate interfacial interaction, which also led to the formation of the most surface synergetic oxygen vacancies (SSOV, Pt^{2+}−O_v−$Mn^{\delta+}$). Pt/OMS-2−3 showed excellent catalytic activity toward oxidation toluene, as well as long-term thermal stability and water vapor resistance. The results of toluene-TPD and *in situ* DRIFTS experiments further confirmed that more reactive oxygen species produced by SSOV could promote the deep oxidation of toluene. The result of this study provided a new perspective for the controlled adjustment of Pt size on Pt-based catalysts and the design of highly efficient catalysts for the deep purification of toluene.

ASSOCIATED CONTENT

Supporting Information

The Supporting Information is available free of charge at https://pubs.acs.org/doi/10.1021/acs.langmuir.3c01734.

The detailed experimental procedures; characterization data of N_2 adsorption−desorption, TEM and HRTEM of OMS-2, Raman spectra, TEM and XPS of Pt/OMS-2−3 before and after reaction, and *in situ* DRIFTS of Pt/OMS-2−2 (PDF)

AUTHOR INFORMATION

Corresponding Author

Haiqin Wan − *State Key Laboratory of Pollution Control and Resource Reuse, School of Environment, Center of Modern Analysis, Jiangsu Key Laboratory of Vehicle Emissions Control, Nanjing University, Nanjing 210023, P. R. China;* orcid.org/0000-0003-0639-4576; Email: wanhq@nju.edu.cn

Authors

Lixin Zhang − *State Key Laboratory of Pollution Control and Resource Reuse, School of Environment, Center of Modern Analysis, Jiangsu Key Laboratory of Vehicle Emissions Control, Nanjing University, Nanjing 210023, P. R. China*

Linjun Zhong − *State Key Laboratory of Pollution Control and Resource Reuse, School of Environment, Center of Modern Analysis, Jiangsu Key Laboratory of Vehicle Emissions Control, Nanjing University, Nanjing 210023, P. R. China*

Pinhua Yu − *Research Institute of Sinopec Nanjing Chemical Industry Co. Ltd., Nanjing 210048, P. R. China*

Haitao Li − *Department of Science and Technology Development, Sinopec Nanjing Chemical Industry Co. Ltd., Nanjing 210048, P. R. China*

Zhou Zhou − *College of Environmental Science and Engineering, Yangzhou University, Yangzhou 225127 Jiangsu, P. R. China*

Qing Tong − *State Key Laboratory of Pollution Control and Resource Reuse, School of Environment, Center of Modern Analysis, Jiangsu Key Laboratory of Vehicle Emissions Control, Nanjing University, Nanjing 210023, P. R. China*

Lin Dong − *State Key Laboratory of Pollution Control and Resource Reuse, School of Environment, Center of Modern Analysis, Jiangsu Key Laboratory of Vehicle Emissions Control, Nanjing University, Nanjing 210023, P. R. China;* orcid.org/0000-0002-8393-6669

Complete contact information is available at: https://pubs.acs.org/10.1021/acs.langmuir.3c01734

Notes

The authors declare no competing financial interest.

ACKNOWLEDGMENTS

This work was supported by financial support from the National Natural Science Foundation of China (21976082 and 22106067).

REFERENCES

(1) Lin, Q.; Gao, Z.; Zhu, W.; Chen, J.; An, T. Underestimated contribution of fugitive emission to VOCs in pharmaceutical industry based on pollution characteristics, odorous activity and health risk assessment. *J. Environ. Sci.* **2023**, *126*, 722−733.

(2) He, C.; Cheng, J.; Zhang, X.; Douthwaite, M.; Pattisson, S.; Hao, Z. Recent Advances in the Catalytic Oxidation of Volatile Organic Compounds: A Review Based on Pollutant Sorts and Sources. *Chem. Rev.* **2019**, *119*, 4471−4568.

(3) Liu, Y.; Li, S.; Wang, Q.; Zheng, X.; Zhao, Y.; Lu, W. Occupational health risks of VOCs emitted from the working face of municipal solid waste landfill: Temporal variation and influencing factors. *Waste Manage.* **2023**, *160*, 173−181.

(4) Zhang, X.; Gao, B.; Creamer, A. E.; Cao, C.; Li, Y. Adsorption of VOCs onto engineered carbon materials: A review. *J. Hazard. Mater.* **2017**, *338*, 102−123.

(5) Liu, L.; Shao, G.; Ma, C.; Nikiforov, A.; De Geyter, N.; Morent, R. Plasma-catalysis for VOCs decomposition: A review on micro- and macroscopic modeling. *J. Hazard. Mater.* **2023**, *451*, No. 131100.

(6) Yue, X.; Ma, N. L.; Sonne, C.; Guan, R.; Lam, S. S.; Van Le, Q.; Chen, X.; Yang, Y.; Gu, H.; Rinklebe, J.; Peng, W. Mitigation of indoor air pollution: A review of recent advances in adsorption materials and catalytic oxidation. *J. Hazard. Mater.* **2021**, *405*, No. 124138.

(7) Guo, Y.; Wen, M.; Li, G.; An, T. Recent advances in VOC elimination by catalytic oxidation technology onto various nanoparticles catalysts: a critical review. *Appl. Catal., B* **2021**, *281*, No. 119447.

(8) Shi, Y.; Li, Z.; Wang, J.; Zhou, R. Synergistic effect of Pt/Ce and USY zeolite in Pt-based catalysts with high activity for VOCs degradation. *Appl. Catal., B* **2021**, *286*, No. 119936.

(9) Huang, Z.; Cao, S.; Yu, J.; Tang, X.; Guo, Y.; Guo, Y.; Wang, L.; Wang, L.; Dai, S.; Dai, S.; Zhan, W. Total Oxidation of Light Alkane over Phosphate-Modified Pt/CeO_2 Catalysts. *Environ. Sci. Technol.* **2022**, *56*, 9661−9671.

(10) Peng, H.; Dong, T.; Zhang, L.; Wang, C.; Liu, W.; Bao, J.; Wang, X.; Zhang, N.; Wang, Z.; Wu, P.; Zhang, P.; Dai, S. Active and stable Pt-Ceria nanowires@silica shell catalyst: Design, formation mechanism and total oxidation of CO and toluene. *Appl. Catal., B* **2019**, *256*, No. 117807.
(11) Wang, Z.; Ma, P.; Zheng, K.; Wang, C.; Liu, Y.; Dai, H.; Wang, C.; His, H. C.; Deng, J. Size effect, mutual inhibition and oxidation mechanism of the catalytic removal of a toluene and acetone mixture over TiO_2 nanosheet-supported Pt nanocatalysts. *Appl. Catal., B* **2020**, *274*, No. 118963.
(12) Shi, Y.; Wang, J.; Zhou, R. Pt-support interaction and nanoparticle size effect in Pt/CeO_2-TiO_2 catalysts for low temperature VOCs removal. *Chemosphere* **2021**, *265*, No. 129127.
(13) Yuan, Z.; Chen, Z.; Mao, J.; Zhou, R. The size effect and high activity of nanosized platinum supported catalysts for low temperature oxidation of volatile organic compounds. *Chin. J. Chem. Eng.* **2021**, *39*, 135−143.
(14) Chen, C.; Chen, F.; Zhang, L.; Pan, S.; Bian, C.; Zheng, X.; Meng, X.; Xiao, F. S. Importance of platinum particle size for complete oxidation of toluene over Pt/ZSM-5 catalysts. *Chem. Commun.* **2015**, *51*, 5936−5938.
(15) Shi, Y.; Wan, J.; Kong, F.; Wang, Y.; Zhou, R. Influence of Pt dispersibility and chemical states on catalytic performance of Pt/CeO_2-TiO_2 catalysts for VOCs low-temperature removal. *Colloids Surf., A* **2022**, *652*, No. 129932.
(16) Xu, Z.; Mo, S.; Li, Y.; Zhang, Y.; Wu, J.; Fu, M.; Niu, X.; Hu, Y.; Ye, D. Pt/MnO_x for toluene mineralization via ozonation catalysis at low temperature: SMSI optimization of surface oxygen species. *Chemosphere* **2022**, *286*, No. 131754.
(17) Peng, R.; Li, S.; Sun, X.; Ren, Q.; Chen, L.; Fu, M.; Wu, J.; Ye, D. Size effect of Pt nanoparticles on the catalytic oxidation of toluene over Pt/CeO_2 catalysts. *Appl. Catal., B* **2018**, *220*, 462−470.
(18) Yu, K.; Deng, J.; Shen, Y.; Wang, A.; Shi, L.; Zhang, D. Efficient catalytic combustion of toluene at low temperature by tailoring surficial Pt^0 and interfacial Pt-Al$(OH)_x$ species. *iScience* **2021**, *24*, No. 102689.
(19) Cheng, Z.; Feng, B.; Chen, Z.; Zheng, J.; Li, J.; Zuo, S. La_2O_3 modified silica-pillared clays supported PtO_x nanocrystalline catalysts for catalytic combustion of benzene. *Chem. Eng. J.* **2020**, *392*, No. 123747.
(20) Chen, J.; Jiang, M.; Xu, W.; Chen, J.; Hong, Z.; Jia, H. Incorporating Mn cation as anchor to atomically disperse Pt on TiO_2 for low-temperature removal of formaldehyde. *Appl. Catal., B* **2019**, *259*, No. 118013.
(21) Li, D.; Yu, Q.; Li, S. S.; Wan, H. Q.; Liu, L. J.; Qi, L.; Liu, B.; Gao, F.; Dong, L.; Chen, Y. W. The remarkable enhancement of CO-pretreated CuO-Mn_2O_3/gamma-Al_2O_3 supported catalyst for the reduction of NO with CO: the formation of surface synergetic oxygen vacancy. *Chem. − Eur. J.* **2011**, *17*, 5668−5679, DOI: 10.1002/chem.201002786.
(22) Xiong, Y.; Yao, X.; Tang, C.; Zhang, L.; Cao, Y.; Deng, Y.; Gao, F.; Dong, L. Effect of CO-pretreatment on the CuO-V_2O_5/γ-Al_2O_3 catalyst for NO reduction by CO. *Catal. Sci. Technol.* **2014**, *4*, 4416−4425.
(23) Tan, W.; Cai, Y.; Xie, S.; Xu, J.; Ma, K.; Ye, K.; Ma, L.; Ehrlich, S. N.; Zou, W.; Gao, F.; Dong, L.; Liu, F. Constructing efficient CuO-CeO_2 catalyst for NO reduction by CO: New insights into the structure-activity relationship. *Chem. Eng. J.* **2023**, *456*, No. 140807.
(24) Li, S.; Chen, X.; Wang, F.; Xie, Z.; Hao, Z.; Liu, L.; Shen, B. Promotion effect of Ni doping on the oxygen resistance property of Fe/CeO_2 catalyst for CO-SCR reaction: Activity test and mechanism investigation. *J. Hazard. Mater.* **2022**, *431*, No. 128622.
(25) Yan, L.; Wang, Q.; Qu, W.; Yan, T.; Li, H.; Wang, P.; Zhang, D. Tuning $Ti^{\delta+}$-Vo··-$Pt^{\delta+}$ interfaces over Pt/TiO_2 catalysts for efficient photocatalytic oxidation of toluene. *Chem. Eng. J.* **2022**, *431*, No. 134209.
(26) Zhang, L.; Zhu, Z.; Tan, W.; Ji, J.; Cai, Y.; Tong, Q.; Xiong, Y.; Wan, H.; Dong, L. Thermal-Driven Optimization of the Strong Metal-Support Interaction of a Platinum-Manganese Oxide Octahedral Molecular Sieve to Promote Toluene Oxidation: Effect of the Interface Pt^{2+}-O_v-$Mn^{\delta+}$. *ACS Appl. Mater. Interfaces* **2022**, *14*, 56790−56800.
(27) Quinson, J.; Inaba, M.; Neumann, S.; Swane, A. A.; Bucher, J.; Simonsen, S. B.; Theil Kuhn, L.; Kirkensgaard, J. J. K.; Jensen, K. M. O.; Oezaslan, M.; Kunz, S.; Arenz, M. Investigating Particle Size Effects in Catalysis by Applying a Size-Controlled and Surfactant-Free Synthesis of Colloidal Nanoparticles in Alkaline Ethylene Glycol: Case Study of the Oxygen Reduction Reaction on Pt. *ACS Catal.* **2018**, *8*, 6627−6635.
(28) Su, J.; Cheng, C.; Guo, Y.; Xu, H.; Ke, Q. OMS-2-based catalysts with controllable hierarchical morphologies for highly efficient catalytic oxidation of formaldehyde. *J. Hazard. Mater.* **2019**, *380*, No. 120890.
(29) Iyer, A.; Galindo, H.; Sithambaram, S.; King'ondu, C.; Chen, C. H.; Suib, S. L. Nanoscale manganese oxide octahedral molecular sieves (OMS-2) as efficient photocatalysts in 2-propanol oxidation. *Appl. Catal., A* **2010**, *375*, 295−302.
(30) Cheng, S.; Yang, L.; Chen, D.; Ji, X.; Jiang, Z.-j.; Ding, D.; Liu, M. Phase evolution of an alpha MnO_2-based electrode for pseudocapacitors probed by in operando Raman spectroscopy. *Nano Energy* **2014**, *9*, 161−167.
(31) Yang, S.; Zhao, H.; Dong, F.; Tang, Z.; Zha, F. Three-dimensional flower-like OMS-2 supported Ru catalysts for application in the combustion reaction of o-dichlorobenzene. *Catal. Sci. Technol.* **2019**, *9*, 6503−6516.
(32) Zhang, D.; Zhang, L.; Shi, L.; Fang, C.; Li, H.; Gao, R.; Huang, L.; Zhang, J. In-situ supported MnO_x-CeO_x on carbon nanotubes for the low-temperature selective catalytic reduction of NO with NH_3. *Nanoscale* **2013**, *5*, 1127−1136.
(33) Lu, Y.; Deng, H.; Pan, T.; Liao, X.; Zhang, C.; He, H. Effective Toluene Ozonation over delta-MnO_2: Oxygen Vacancy-Induced Reactive Oxygen Species. *Environ. Sci. Technol.* **2023**, *57*, 2918−2927.
(34) He, C.; Liao, Y.; Chen, C.; Xia, D.; Wang, Y.; Tian, S.; Yang, J.; Shu, D. Realizing a redox-robust Ag/MnO_2 catalyst for efficient wet catalytic ozonation of S-VOCs: Promotional role of Ag(0)/Ag(I)-Mn based redox shuttle. *Appl. Catal., B* **2022**, *303*, No. 120881.
(35) Hu, Z.; Liu, X.; Meng, D.; Guo, Y.; Guo, Y.; Lu, G. Effect of Ceria Crystal Plane on the Physicochemical and Catalytic Properties of Pd/Ceria for CO and Propane Oxidation. *ACS Catal.* **2016**, *6*, 2265−2279.
(36) Yang, W.; Su, Z.; Xu, Z.; Yang, W.; Peng, Y.; Li, J. Comparative study of α-, β-, γ- and δ-MnO_2 on toluene oxidation: Oxygen vacancies and reaction intermediates. *Appl. Catal., B* **2020**, *260*, No. 118150.
(37) Wang, F.; Deng, J.; Impeng, S.; Shen, Y.; Yan, T.; Chen, G.; Shi, L.; Zhang, D. Unraveling the effects of the coordination number of Mn over α-MnO_2 catalysts for toluene oxidation. *Chem. Eng. J.* **2020**, *396*, No. 125192.
(38) Xiao, M.; Han, D.; Yang, X.; Tsona Tchinda, N.; Du, L.; Guo, Y.; Wei, Y.; Yu, X.; Ge, M. Ni-doping-induced oxygen vacancy in Pt-CeO_2 catalyst for toluene oxidation: Enhanced catalytic activity, water-resistance, and SO_2-tolerance. *Appl. Catal., B* **2023**, *323*, No. 122173.
(39) Kondratowicz, T.; Drozdek, M.; Michalik, M.; Gac, W.; Gajewska, M.; Kuśtrowski, P. Catalytic activity of Pt species variously dispersed on hollow ZrO_2 spheres in combustion of volatile organic compounds. *Appl. Surf. Sci.* **2020**, *513*, No. 145788.
(40) Tan, W.; Xie, S.; Cai, Y.; Wang, M.; Yu, S.; Low, K. B.; Li, Y.; Ma, L.; Ehrlich, S. N.; Gao, F.; Dong, L.; Liu, F. Transformation of Highly Stable Pt Single Sites on Defect Engineered Ceria into Robust Pt Clusters for Vehicle Emission Control. *Environ. Sci. Technol.* **2021**, *55*, 12607−12618.
(41) Chen, L.; Liu, Y.; Fang, X.; Cheng, Y. Simple strategy for the construction of oxygen vacancies on alpha-MnO_2 catalyst to improve toluene catalytic oxidation. *J. Hazard. Mater.* **2021**, *409*, No. 125020.
(42) Nie, L.; Mei, D.; Xiong, H.; Peng, B.; Ren, Z.; Pereira-Hernandez, X. I.; DeLaRiva, A.; Wang, M.; Engelhard, M. H.; Kovarik, L.; Datye, A. K.; Wang, Y. Activation of surface lattice oxygen

in single-atom Pt/CeO_2 for low-temperature CO oxidation. *Science* **2017**, *358*, 1419−1423.
(43) Chen, X.; Chen, X.; Yu, E.; Cai, S.; Jia, H.; Chen, J.; Liang, P. In-situ pyrolysis of Ce-MOF to prepare CeO_2 catalyst with obviously improved catalytic performance for toluene combustion. *Chem. Eng. J.* **2018**, *344*, 469−479.
(44) Wang, Y.; Wu, J.; Wang, G.; Yang, D.; Ishihara, T.; Guo, L. Oxygen vacancy engineering in Fe doped akhtenskite-type MnO_2 for low-temperature toluene oxidation. *Appl. Catal., B* **2021**, *285*, No. 119873.
(45) Yu, E.; Li, J.; Chen, J.; Chen, J.; Hong, Z.; Jia, H. Enhanced photothermal catalytic degradation of toluene by loading Pt nanoparticles on manganese oxide: Photoactivation of lattice oxygen. *J. Hazard. Mater.* **2020**, *388*, No. 121800.
(46) Li, S.; Lin, Y.; Wang, D.; Zhang, C.; Wang, Z.; Li, X. Polyhedral cobalt oxide supported Pt nanoparticles with enhanced performance for toluene catalytic oxidation. *Chemosphere* **2021**, *263*, No. 127870.
(47) Boronin, A. I.; Slavinskaya, E. M.; Figueroba, A.; Stadnichenko, A. I.; Kardash, T. Y.; Stonkus, O. A.; Fedorova, E. A.; Muravev, V. V.; Svetlichnyi, V. A.; Bruix, A.; Neyman, K. M. CO oxidation activity of Pt/CeO_2 catalysts below 0 °C: platinum loading effects. *Appl. Catal., B* **2021**, *286*, No. 119931.
(48) Wei, X.; Li, K.; Zhang, X.; Tong, Q.; Ji, J.; Cai, Y.; Gao, B.; Zou, W.; Dong, L. CeO_2 nanosheets with anion-induced oxygen vacancies for promoting photocatalytic toluene mineralization: Toluene adsorption and reactive oxygen species. *Appl. Catal., B* **2022**, *317*, No. 121694.
(49) Zhang, X.; Bi, F.; Zhu, Z.; Yang, Y.; Zhao, S.; Chen, J.; Lv, X.; Wang, Y.; Xu, J.; Liu, N. The promoting effect of H_2O on rod-like $MnCeO_x$ derived from MOFs for toluene oxidation: A combined experimental and theoretical investigation. *Appl. Catal., B* **2021**, *297*, No. 120393.
(50) Pan, T.; Deng, H.; Lu, Y.; Ma, J.; Wang, L.; Zhang, C.; He, H. Synergistic Catalytic Oxidation of Typical Volatile Organic Compound Mixtures on Mn-Based Catalysts: Significant Promotion Effect and Reaction Mechanism. *Environ. Sci. Technol.* **2023**, *57*, 1123−1133.
(51) Chen, P.; Cui, W.; Wang, H.; Dong, Xa.; Li, J.; Sun, Y.; Zhou, Y.; Zhang, Y.; Dong, F. The importance of intermediates ring-opening in preventing photocatalyst deactivation during toluene decomposition. *Appl. Catal., B* **2020**, *272*, No. 118977.
(52) Feng, Y.; Dai, L.; Wang, Z.; Peng, Y.; Duan, E.; Liu, Y.; Jing, L.; Wang, X.; Rastegarpanah, A.; Dai, H.; Deng, J. Photothermal Synergistic Effect of Pt_1/CuO-CeO_2 Single-Atom Catalysts Significantly Improving Toluene Removal. *Environ. Sci. Technol.* **2022**, *56*, 8722−8732.
(53) Dong, X.; Cui, W.; Wang, H.; Li, J.; Sun, Y.; Wang, H.; Zhang, Y.; Huang, H.; Dong, F. Promoting ring-opening efficiency for suppressing toxic intermediates during photocatalytic toluene degradation via surface oxygen vacancies. *Sci. Bull.* **2019**, *64*, 669−678.
(54) Hong, W.; Liu, Y.; Zhu, T.; Wang, H.; Sun, Y.; Shen, F.; Li, X. Promoting the Catalytic Ozonation of Toluene by Introducing SO_4^{2-} into the alpha-MnO_2/ZSM-5 Catalyst to Tune Both Oxygen Vacancies and Acid Sites. *Environ. Sci. Technol.* **2022**, *56*, 15695−15704.
(55) Wenig, R. W.; Schrader, G. L. In-Situ FTIR Study of n-Butane Selective Oxidation to Maleic Anhydride on V-P-O Catalysts. *J. Phys. Chem. C* **1986**, *90*, 6480−6488.
(56) Yang, L.; Liu, Q.; Han, R.; Fu, K.; Su, Y.; Zheng, Y.; Wu, X.; Song, C.; Ji, N.; Lu, X.; Ma, D. Confinement and synergy effect of bimetallic Pt-Mn nanoparticles encapsulated in ZSM-5 zeolite with superior performance for acetone catalytic oxidation. *Appl. Catal., B* **2022**, *309*, No. 121224.
(57) Wang, Z.; Zhang, L.; Ji, J.; Wu, Y.; Cai, Y.; Yao, X.; Gu, X.; Xiong, Y.; Wan, H.; Dong, L.; Chen, Y. W. Catalytic enhancement of small sizes of CeO_2 additives on Ir/Al_2O_3 for toluene oxidation. *Appl. Surf. Sci.* **2022**, *571*, No. 151200.

https://doi.org/10.1021/acs.langmuir.3c01734
Langmuir 2023, 39, 13620−13629